Entanglement detection and quantum metrology by Raman photon-diffraction imaging

Hongyi Yu and Wang Yao*

Department of Physics and Center of Theoretical and Computational Physics, The University of Hong Kong, Hong Kong, China

(Received 22 June 2012; published 2 April 2013)

We show that far-field diffraction images of spontaneously scattered Raman photons can be used for detection of spin entanglement and for metrology of field gradients in cold atomic ensembles. For many-body states with small or maximum uncertainty in the spin-excitation number, entanglement is simply witnessed by the presence of a sharp diffraction peak or dip. The gradient vector of external fields is measured by the displacement of a diffraction peak due to inhomogeneous spin precession, which suggests a possibility for precision measurements beyond the standard quantum limit without entanglement. Monitoring of the temporal decay of the diffraction peak can also realize a nondemolition probe of the temperature and collisional interactions in trapped cold atomic gases. The approach can be readily generalized to cold molecules, trapped ions, and solid-state spin ensembles.

DOI: 10.1103/PhysRevA.87.042303 PACS number(s): 03.67.Bg, 03.67.Mn, 06.20.−f, 42.25.Fx

I. INTRODUCTION

Cold atomic ensembles offer an ideal platform for the study of quantum many-body physics and for the implementation of quantum information processing [1]. With entanglement speculated to be a key phenomenon on these occasions, an efficient approach to the detection of entanglement is crucial for understanding its profound roles [2]. The spin of cold atoms is also widely used for precision measurements of external fields. A topic of current interest is quantum metrology, which utilizes quantum properties and particularly entanglement in the probe system to reach measurement sensitivity beyond the standard quantum limit (SQL) [3].

To address these outstanding demands in the exploration of quantum physics and quantum technology using cold atomic ensembles, the key is efficient access to the right piece of information in the spin subspace. An ideal interface between spin and photon is offered by the process of spontaneous Stokes scattering [4–13]: with a laser driving an ensemble of atoms in the Λ configuration, a collective spin excitation can be spontaneously converted into a Stokes photon with phase and wave vector preserved. One may thus anticipate that the photon-diffraction pattern can provide information on collective spin properties. Earlier studies on the diffraction of collectively emitted photons have focused on the super-radiance phenomenon (i.e., induced directional coherent radiation) in very dense atomic ensembles [14–16], or in ensembles prepared with a single excitation [17–21].

In this paper, we show that the far-field diffraction image of spontaneously emitted Raman photons can be used for detection of spin entanglement and for precision measurements of the gradient vector of external fields in cold atomic ensembles. We find that the strength of a sharp diffraction peak or dip measures the sum of the spin pair correlations and detects entanglement through pair-correlation sum rules that we derive from optimal spin-squeezing inequalities [22–25]. For many-body states with small or maximum uncertainty in the spin-excitation number, entanglement is simply witnessed by the presence of the peak or dip. Inhomogeneous spin precessions in a field gradient lead to displacement of the diffraction peak (dip), which can serve as a principle for vector metrology of fields gradients and for calibration of inhomogeneity in optical lattices. The gradiometer sensitivity can reach $1/N$ by using a spin-coherent-state of N unentangled atoms as the probe, which suggests a possibility for going beyond the SQL of $1/\sqrt{N}$ without entanglement [26–29]. Motional dynamics leads to temporal decay of the diffraction peak which can be used for a nondemolition probe of the temperature and collisional interactions in trapped atomic gases.

Two remarkable features make this approach particularly suitable for ensembles with large numbers of atoms. First, regardless of the ensemble size, the spin-dephasing noise as a major error source results only in decay of the peak (dip) strength on a time scale equal to the dephasing time of a single spin. Second, the number of useful photons from a single copy of a many-body state can be as large as its spin-excitation number for cold atomic ensembles, which are typically dilute (i.e., with interatomic distance comparable to or larger than the optical wavelength). This approach complements existing optical methods for probing many-body quantum states [30–36], and is readily applicable in other systems including molecular ensembles, trapped ions, and solid-state spin ensembles.

The rest of the paper is organized as follows. In Sec. II, we analyze the the far-field diffraction pattern of Raman photons and show how to extract the pair-correlation sum of the atomic spins. In Sec. III, we derive pair-correlation sum rules for detecting entanglement. In Sec. IV, we analyze the time evolution of the diffraction pattern from dilute ensembles. In Sec. V, we discuss the use of the diffraction pattern for precision measurements of the field gradient and for a nondemolition probe of the atomic motion and temperature. Section VI is a brief summary of the paper. Additional supplementary details on the derivations are grouped in the Appendices.

II. DIFFRACTION PATTERN OF STOKES PHOTONS

Consider an optically thin cold atomic ensemble with a Λ level configuration where two atomic ground states $|g\rangle$ and $|s\rangle$ can be optically coupled to a common excited state $|e\rangle$ (Fig. 1, inset). The ensemble is driven by a laser with Rabi frequency Ω_L, detuning Δ, and wave vector $\mathbf{k}_0 = k_0\hat{\mathbf{z}}$. We assume that the atomic motion can be taken as frozen for the

*wangyao@hku.hk

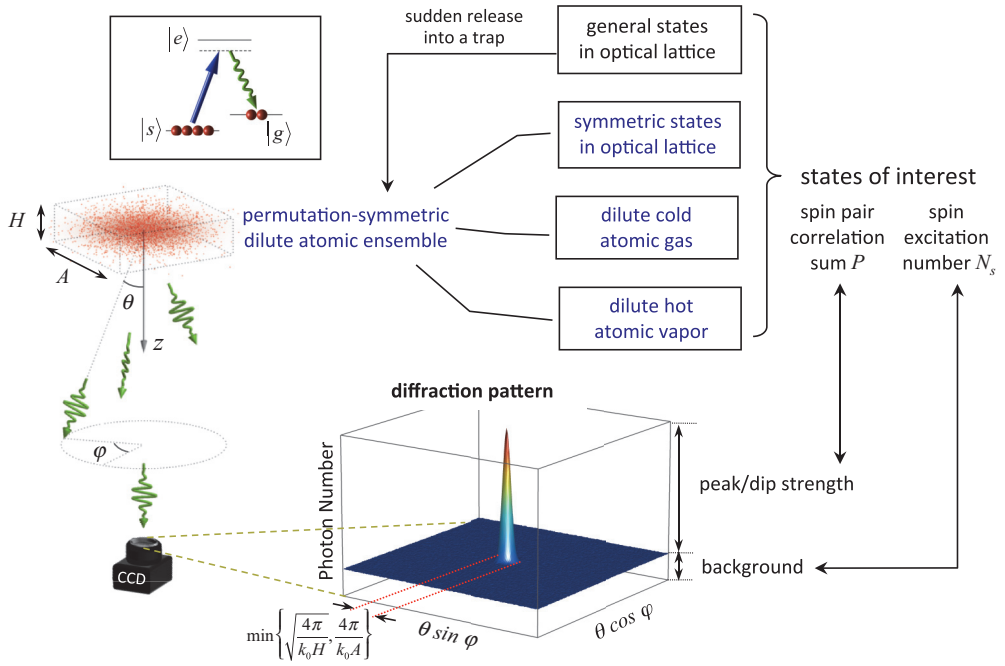

FIG. 1. (Color online) Far-field diffraction image of Stokes photons from permutation-symmetric dilute ensembles. The pair-correlation sum P in the many-atom state of interest manifests as a sharp diffraction peak (for $P > 0$) or dip (for $P < 0$) along the forward direction, with strength proportional to $|P|$ and width inversely proportional to the ensemble size.

duration of photon emission. With the laser coupling the $|s\rangle$ to $|e\rangle$ transition, an atom can go from state $|s\rangle$ to $|g\rangle$ by emitting a Stokes photon into the vacuum. When Δ is much larger than Ω_L and the excited state's homogeneous linewidth Γ_0, $|e\rangle$ can be adiabatically eliminated, leading to the effective light-atom coupling in the electric-dipole and rotating-wave approximations:

$$\hat{H} = \sum_{\mathbf{k}} \hbar\omega_k \hat{a}^\dagger_{\mathbf{k}} \hat{a}_{\mathbf{k}} + \sum_j E_z \hat{\sigma}^z_j + \sum_{\mathbf{k}} g_{\mathbf{k}} \sum_j e^{-i(\mathbf{k}-\mathbf{k}_0)\cdot\mathbf{r}_j} \hat{\sigma}^-_j \hat{a}^\dagger_{\mathbf{k}} + \text{H.c.} \quad (1)$$

Here $g_{\mathbf{k}} = \frac{\Omega_L}{2\Delta}\sqrt{\frac{2\pi\omega_k}{V}}\hat{\mathbf{e}}_{\mathbf{k}} \cdot \boldsymbol{\mu}$, $\hat{\mathbf{e}}_{\mathbf{k}}$ and $\boldsymbol{\mu}$ being respectively the unit polarization vector and the single-atom dipole. $\hat{\sigma}^-_j \equiv |g\rangle_j\langle s|$ and $\hat{\sigma}^z_j \equiv |s\rangle_j\langle s| - |g\rangle_j\langle g|$. We assume that anti-Stokes scattering is either forbidden by the polarization selection rule or suppressed by the much larger detuning when $E_z \gg \hbar\Delta$.

Emission of a Stokes photon into mode $\mathbf{k} = (k,\theta,\varphi)$ is accompanied by the annihilation of a spin excitation by $\hat{J}^-(\Delta\mathbf{k}) \equiv \sum_{j=1}^N e^{-i\Delta\mathbf{k}\cdot\mathbf{r}_j}\hat{\sigma}^-_j$, $\Delta\mathbf{k} = \mathbf{k} - \mathbf{k}_0$. The angular distribution of the photon emission rate is given by $I(\theta,\varphi,t) = I_s(\theta)I_c(\theta,\varphi,t)$. I_s is the single-atom dipole emission pattern, a slowly varying function of θ. $I_c(\theta,\varphi,t) \equiv \text{Tr}[\hat{J}^+(\Delta\mathbf{k})\hat{J}^-(\Delta\mathbf{k})\rho(t)]$ is a collective factor where $\rho(t)$ is the atomic density matrix. At the initial time of photon emission,

$$I_c(\theta,\varphi,0) = \langle\hat{N}_s\rangle + \sum_{j\neq j'} e^{-i\Delta\mathbf{k}\cdot(\mathbf{r}_j-\mathbf{r}_{j'})}\langle\hat{\sigma}^+_{j'}\hat{\sigma}^-_j\rangle = \langle\hat{N}_s\rangle - \frac{P}{N-1} + P\frac{\left|\langle\sum_j e^{-i\Delta\mathbf{k}\cdot\mathbf{r}_j}\rangle\right|^2}{N^2-N}, \quad (2)$$

where $\hat{N}_s \equiv \sum_j(\hat{\sigma}^z_j + 1)/2$ is the spin-excitation number operator. Here and hereafter $\langle\cdots\rangle$ denotes the expectation value over $\rho(0)$, the initial many-body state of interest. $P \equiv \langle\sum_{j\neq j'}\hat{\sigma}^+_{j'}\hat{\sigma}^-_j\rangle$ is the sum of spin pair correlations. The last equals sign in Eq. (2) holds when $\rho(0)$ is invariant under permutation of atoms, which is the typical situation for atom gases. $|\langle\sum_j e^{-i\Delta\mathbf{k}\cdot\mathbf{r}_j}\rangle|^2$ is a sharp feature which equals N^2 along the forward direction ($\theta = 0$) and drops to zero for $\theta \geqslant \theta_b \equiv \min\{\sqrt{\frac{\pi}{k_0 H}}, \frac{2\pi}{k_0 A}\}$ where A and H are respectively the transverse and longitudinal sizes of the ensemble (Fig. 1). Thus, a positive (negative) pair-correlation sum manifests as a sharp diffraction peak (dip), and its magnitude can be read out from the ratio of the peak (dip) to the background:

$$\frac{I(\theta=0) - I(\theta_b)}{I(\theta_b)} = \frac{P}{\langle\hat{N}_s\rangle - P/N}. \quad (3)$$

For general states in optical lattices without permutation symmetry, P can be measured after sudden release of atoms into a spin-independent trap [1]. The density matrix averaged over many ensemble copies will become permutation symmetric after atoms lose memory of their initial positions, while P is preserved by the atomic motions. Moreover, we find that the pair-correlation sum of a dilute hot atomic vapor can be measured in the same way if Stokes photon emission is controlled to be much slower than the atomic motions (see the last part of Appendix A).

III. ENTANGLEMENT DETECTION

The pair-correlation sum measured from the peak- (dip-) to-background ratio [Eq. (3)] can detect entanglement via spin-squeezing inequalities [22–25]. The longitudinal component

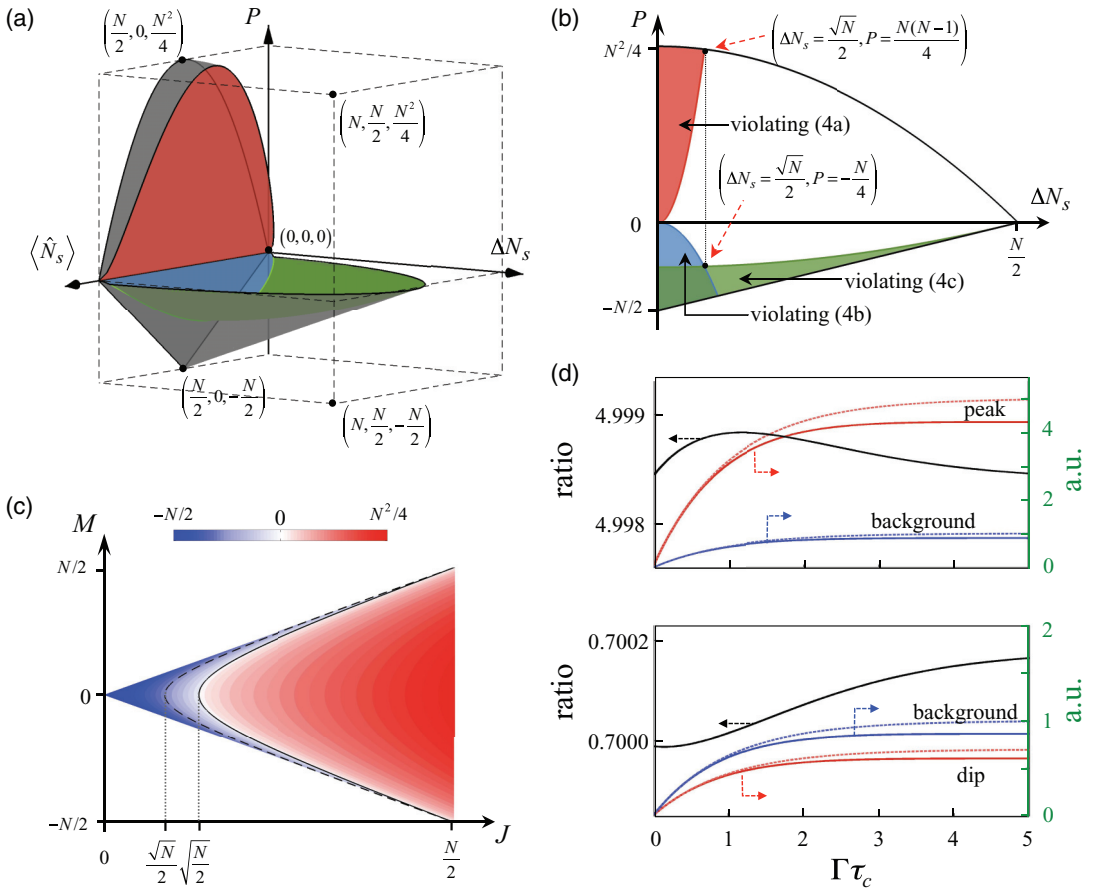

FIG. 2. (Color online) (a) Phase diagram in the parameter space $(\langle\hat{N}_s\rangle, \Delta N_s, P)$. States in the surrounded region are all entangled ones. (b) A slice of (a) taken for $\langle\hat{N}_s\rangle = N/2$. The red, blue, and green regions are entangled states violating inequalities (4a), (4b), and (4c), respectively. The gray surfaces in (a) and the black curves in (b) are boundaries between physical and unphysical regions. Positive and negative sections of the P axis use different linear scales. (c) Strength of the diffraction peak (red) or dip (blue) for eigenstates of total spin $\hat{J}^2$ and $\hat{J}_z$. Inequalities (4a) and (4b) are violated in the peak and dip regions, respectively. States violating inequality (4c) form a subset of the dip region, to the left of the dashed curve. (d) Upper (lower): Peak- (dip-) to-background ratio as a function of the collection interval τ_c for a half-spin-excitation state with $P = 2.5N$ ($P = -0.35N$), shown as the black curve. The calculation is for $N = 4000$ atoms of a two-dimensional (2D) Gaussian distribution with FWHM $A = 100\ \mu$m. Peak or dip (background) strength is evaluated at $\theta = 0$ ($\theta = 2\pi/k_0 A$), shown by the red (blue) solid curve. Dashed curves are calculations with the multiple light scattering and dipole-dipole interaction neglected.

of the total spin is equivalent to the spin-excitation number, $\hat{N}_s \equiv \hat{J}_z + N/2$, and the second moment of the transverse component is equivalent to the pair-correlation sum, $\langle\hat{J}_x^2\rangle + \langle\hat{J}_y^2\rangle = P + N/2$. Many spin-squeezing inequalities derived for first and second moments of the total spin can thus be formulated as pair-correlation sum rules. For example, the optimal spin-squeezing inequalities discovered in Ref. [24] become

$$P \leqslant (N-1)\Delta N_s^2, \tag{4a}$$

$$P \geqslant -\Delta N_s^2, \tag{4b}$$

$$(N-1)P \geqslant \langle\hat{N}_s^2\rangle - N\langle\hat{N}_s\rangle, \tag{4c}$$

where $\Delta N_s \equiv (\langle\hat{N}_s^2\rangle - \langle\hat{N}_s\rangle^2)^{1/2}$. Violation of any one of the inequalities (4a)–(4c) implies entanglement. With the spin-excitation number $\hat{N}_s$ conserved in most physical processes of interest, its expectation value is usually known *a priori*.

ΔN_s can also be measured from the peak- (dip-) to-background ratio in the diffraction image taken after a global rotation of the ensemble. With a $\pi/2$ rotation about an in-plane axis transforming $\hat{J}^x \to \hat{J}^z$ or $\hat{J}^y \to \hat{J}^z$, $\langle\hat{J}_y^2\rangle + \langle\hat{J}_z^2\rangle - N/2$ or $\langle\hat{J}_x^2\rangle + \langle\hat{J}_z^2\rangle - N/2$ can be obtained from the peak- (dip-) to-background ratio in the diffraction image, from which we can solve for ΔN_s.

Entanglement detection based on the above pair-correlation sum rules is described by the phase diagrams shown in Figs. 2(a)–2(c). *Qualitative* criteria become possible for entanglement witnesses in two limits. With vanishing ΔN_s the presence of either a diffraction peak or dip verifies entanglement, while with maximum ΔN_s the presence of a dip verifies entanglement [Figs. 2(a) and 2(b)]. On the other hand, a peak (dip) strength exceeding some threshold value always implies entanglement. Taking half-spin-excitation states for example, observation of a dip-to-background ratio $|r| \geqslant \frac{1}{2}$ or a peak-to-background ratio $r \geqslant \frac{N(N-1)}{N+1}$ verifies entanglement

for any possible ΔN_s. P and ΔN_s can also quantify the entanglement depth in the vicinity of Dicke states [25].

Furthermore, the diffraction image can be used to measure delocalized entanglement as defined in Ref. [37] for atoms in optical lattices. A measure of the bipartite delocalized entanglement at a specified distance $\mathbf{x}$ is given by the entanglement of formation for the delocalized bipartite reduced density operator

$$\rho_{AB}(\mathbf{x}) \equiv \frac{1}{C_{\mathbf{x}}} \sum_{\mathbf{j}} \rho_{\mathbf{j},\mathbf{j}+\mathbf{x}}. \tag{5}$$

Here $C_{\mathbf{x}}$ is the normalization coefficient which corresponds to the number of pairs $\{\mathbf{j},\mathbf{j}+\mathbf{x}\}$. $\rho_{\mathbf{j},\mathbf{j}+\mathbf{x}}$ denotes the two-qubit reduced density matrix deduced from the initial ensemble state $\rho(0)$, where only the sites $\mathbf{j}$ and $\mathbf{j}+\mathbf{x}$ of the lattice are kept while all others are traced out.

As shown in Ref. [37], the lower bound of entanglement of formation for $\rho_{AB}(\mathbf{x})$ can be evaluated from the fidelity $f_\phi(\mathbf{x}) \equiv \langle\phi|\rho_{AB}(\mathbf{x})|\phi\rangle$, with ϕ being one of the four Bell states $\Phi_\pm$ and $\Psi_\pm$. The fidelity is found to be

$$f_{\Phi_\pm}(\mathbf{x}) = \frac{1 - \mathrm{Tr}\left[\sum_{\mathbf{j}} \hat{\sigma}^z_{\mathbf{j}} \hat{\sigma}^z_{\mathbf{j}+\mathbf{x}} \rho(0)\right]}{4} \pm \frac{P_{\mathbf{x}} + P_{-\mathbf{x}}}{2}, \tag{6}$$

where the correlation $P_{\mathbf{x}} \equiv \mathrm{Tr}[\sum_{\mathbf{j}} \hat{\sigma}^+_{\mathbf{j}} \hat{\sigma}^-_{\mathbf{j}+\mathbf{x}} \rho(0)]$. $f_{\Psi_\pm}(\mathbf{x})$ can be obtained from $f_{\Phi_\pm}(\mathbf{x})$ by applying a global unitary transformation.

Equation (2) can be rewritten as $I_c(\theta,\varphi,0) = \langle \hat{N}_s \rangle + \sum_{\mathbf{x}} e^{-i\Delta\mathbf{k}\cdot\mathbf{x}} C_{\mathbf{x}} P_{\mathbf{x}}$. The correlation $P_{\mathbf{x}}$ for arbitrary $\mathbf{x}$ can therefore be obtained through a Fourier transform of the diffraction image. Note that $P_{\mathbf{x}} + P_{-\mathbf{x}} = \mathrm{Tr}[\sum_{\mathbf{j}} (\hat{\sigma}^x_{\mathbf{j}} \hat{\sigma}^x_{\mathbf{j}+\mathbf{x}} + \hat{\sigma}^y_{\mathbf{j}} \hat{\sigma}^y_{\mathbf{j}+\mathbf{x}}) \rho(0)]$. Thus, $\mathrm{Tr}[\sum_{\mathbf{j}} \hat{\sigma}^z_{\mathbf{j}} \hat{\sigma}^z_{\mathbf{j}+\mathbf{x}} \rho(0)]$ can also be obtained by applying a global rotation to all spins to transform $\hat{\sigma}^x \to \hat{\sigma}^z$ or $\hat{\sigma}^y \to \hat{\sigma}^z$.

IV. PERTURBATIVE SOLUTION OF THE ATOMIC EVOLUTION

Hereafter, we focus on dilute ensembles where the interatomic distance is comparable to or larger than the optical wavelength. Remarkably, under this condition, one can collect all Stokes photons, not only those initial ones, for measuring the pair-correlation sum and detecting entanglement in $\rho(0)$.

The diffraction pattern at an arbitrary time is determined by the instantaneous atomic density matrix $\rho(t)$ which differs from $\rho(0)$. As well established in the literature of superradiance [16], the evolution of $\rho(t)$ is described by the Lindblad master equation in the Born-Markov approximation,

$$\begin{aligned} \dot{\rho}(t) &= \mathcal{L}_0\rho(t) + \mathcal{L}_1\rho(t), \\ \mathcal{L}_0\rho &\equiv \frac{\Gamma}{2} \sum_j (2\hat{\sigma}^-_j \rho \hat{\sigma}^+_j - \hat{\sigma}^+_j \hat{\sigma}^-_j \rho - \rho \hat{\sigma}^+_j \hat{\sigma}^-_j), \\ \mathcal{L}_1\rho &\equiv \sum_{j\neq j'} \frac{\Gamma_{jj'}}{2} (2\hat{\sigma}^-_j \rho \hat{\sigma}^+_{j'} - \hat{\sigma}^+_{j'} \hat{\sigma}^-_j \rho - \rho \hat{\sigma}^+_{j'} \hat{\sigma}^-_j) \\ &\quad + i \sum_{j\neq j'} \frac{G_{jj'}}{2} [\hat{\sigma}^+_{j'} \hat{\sigma}^-_j, \rho], \end{aligned} \tag{7}$$

where $\Gamma_{jj'} = \Gamma \frac{\sin(k_0|\mathbf{r}_j - \mathbf{r}_{j'}|)}{k_0|\mathbf{r}_j - \mathbf{r}_{j'}|}$ and $G_{jj'} = \Gamma \frac{\cos(k_0|\mathbf{r}_j - \mathbf{r}_{j'}|)}{k_0|\mathbf{r}_j - \mathbf{r}_{j'}|}$ describe respectively multiple light scattering and the dipole-dipole interaction [16,20]. In the study of super-radiance phenomena in very dense atomic ensembles, these effects must be taken into account nonperturbatively [14]. $\Gamma_{jj'}$ and $G_{jj'}$ drop fast with distance. In dilute atomic ensembles where the atom-atom distance is comparable to or larger than the photon wavelength, the atomic evolution can be solved perturbatively. Using the Laplace transform $w(z) = \int_0^\infty dt e^{-zt} \rho(t)$, we have

$$w(z) = \frac{1}{z - \mathcal{L}_0 - \mathcal{L}_1} \rho(0).$$

For $k_0|\mathbf{r}_j - \mathbf{r}_{j'}| \geqslant 2\pi$, $\mathcal{L}_1$ is small compared to $\mathcal{L}_0$, and we make a perturbative expansion $\frac{1}{z-\mathcal{L}_0-\mathcal{L}_1} = \frac{1}{z-\mathcal{L}_0} + \frac{1}{z-\mathcal{L}_0}\mathcal{L}_1 \frac{1}{z-\mathcal{L}_0} + \cdots$. By inverse Laplace transform we can get the solution of the atomic density matrix $\rho^{(n)}$ keeping up to nth-order effects of $\mathcal{L}_1$.

For the zeroth-order solution $\rho^{(0)}(t) = e^{\mathcal{L}_0 t}\rho(0)$, we find $\mathrm{Tr}[\hat{J}^+(\Delta\mathbf{k})\hat{J}^-(\Delta\mathbf{k})\rho^{(0)}(t)] = e^{-\Gamma t}\mathrm{Tr}[\hat{J}^+(\Delta\mathbf{k})\hat{J}^-(\Delta\mathbf{k})\rho(0)]$, i.e., the initial diffraction pattern is preserved for all time. Comparisons with the exact solution of the master equation for a chain of 12 atoms show that the perturbation expansion converges fast for $k_0|\mathbf{r}_j - \mathbf{r}_{j'}| \geqslant 2\pi$, and the effects of multiple light scattering and the dipole-dipole interaction are well accounted for by keeping only the first-order effects of the $\mathcal{L}_1$ term:

$$\rho^{(1)}(t) = \rho^{(0)}(t) + \int_0^t d\tau e^{\mathcal{L}_0\tau} [\mathcal{L}_1 \rho^{(0)}(t-\tau)].$$

The $\mathcal{L}_1$ term leads to a slowly varying modulation of the diffraction pattern, which barely changes the ratio of the sharp peak (dip) to its neighboring background. Details of this modulation and the convergence check for the perturbative solutions can be found in Appendix A.

Based on this perturbative solution, we analyze the diffraction pattern of Stokes photons as a function of the collection time τ_c. We find that the weak processes of $\mathcal{L}_1$ result in only a slowly varying modulation of the diffraction pattern, barely changing the ratio of the sharp peak or dip to its neighboring background. Namely,

$$r(\tau_c) \equiv \frac{n(\theta=0,\tau_c) - n(\theta_b,\tau_c)}{n(\theta_b,\tau_c)} \cong \frac{P}{\langle \hat{N}_s \rangle - P/N}, \tag{8}$$

where $n(\theta,\varphi,\tau_c) \equiv \delta\Omega \int_0^{\tau_c} dt I(\theta,\varphi,t)$ is the number of photons emitted into an infinitesimal solid angle in the collection interval $0 \leqslant t \leqslant \tau_c$. For a dilute ensemble Eq. (8) holds for arbitrarily large τ_c [cf. Fig. 2(d)]. Thus the pair-correlation sum can be faithfully read out from the diffraction pattern of all photons and is not limited to those initial ones.

We estimate the range of applicability of our treatment. The dilute condition is satisfied by typical cold atom gases of a density 10^{10}–10^{12} cm^{-3} or by atoms in an optical lattice. The duration of Stokes photon emission is on the time scale $\Gamma^{-1} = (\frac{\Omega_L}{2\Delta})^{-2}\Gamma_0^{-1}$. The excited-state decay rate $\Gamma_0 \gtrsim 30\ \mu\mathrm{s}^{-1}$ for typical alkali-metal atoms [6–13]. Taking $(\frac{\Omega_L}{2\Delta})^{-2} \sim 40$, all Stokes photons are emitted on a time scale $\Gamma^{-1} \lesssim \mu$s. For cold atom gases with a temperature of 1–100 μK, the average velocity is 0.01–0.1 m/s. Atoms can travel only 10–100 nm in the duration of Γ^{-1} which is indeed negligible as compared to the light wavelength.

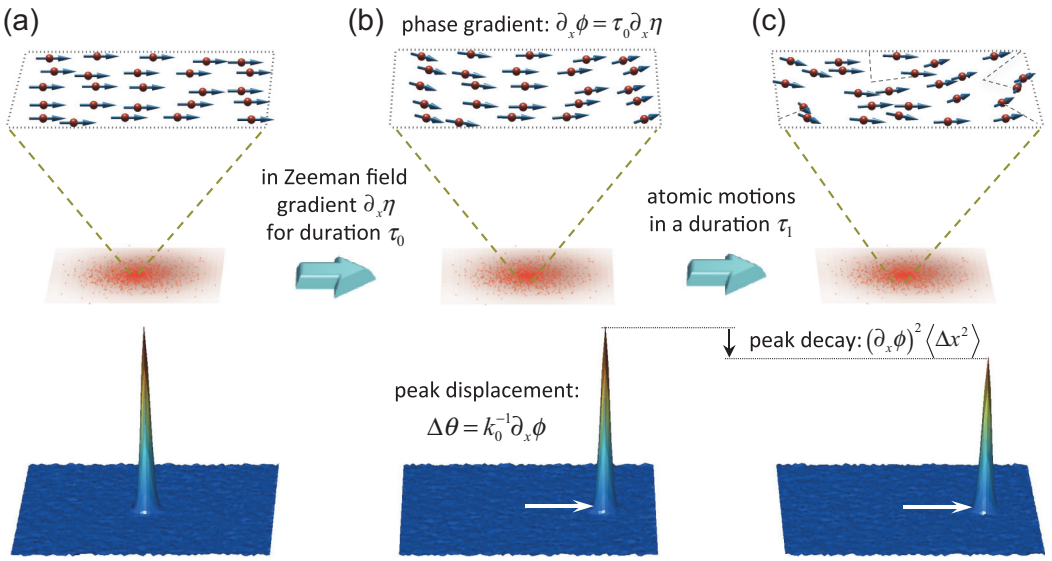

FIG. 3. (Color online) Diffraction images (bottom panels) from atomic ensembles in different spin configurations (top panels). (a) Spin-coherent state with in-plane polarization. (b) Evolution in a Zeeman field gradient; a phase gradient of spins is imprinted, resulting in a displacement of the diffraction peak, which can form the principle of a gradiometer. (c) Atomic motions diminish the spin polarization, resulting in decay of the displaced peak. This can be the principle for nondemolition measurement of the atomic temperature and collisional interactions.

V. FIELD GRADIOMETER AND NONDEMOLITION PROBE OF ATOMIC MOTIONS AND TEMPERATURE

Under free evolution, the pair-correlation changes as $\mathrm{Tr}[\hat{\sigma}_{i'}^{+}\hat{\sigma}_{i}^{-}\rho(\tau)] = e^{i(\eta_i\tau-\eta_{i'}\tau)-2\gamma\tau}\mathrm{Tr}[\hat{\sigma}_{i'}^{+}\hat{\sigma}_{i}^{-}\rho(0)]$, where η_i is the Zeeman frequency and γ the homogeneous dephasing rate of an individual spin. The pair-correlation sum thus decays only at the single-spin dephasing rate. Therefore entanglement in $\rho(0)$ can be reliably detected from the dephased state $\rho(\tau)$ as long as $\tau \ll \gamma^{-1}$, even when the fidelity becomes exponentially small with N [25].

The spatial inhomogeneity of external fields leads to a position-dependent Zeeman frequency $\eta(\mathbf{r})$ and hence inhomogeneous precession of spins. If the size of the ensemble is small compared to the variation length scale of the field, the dominating term is the gradient: $\eta(\mathbf{r}) \cong \mathbf{r}\cdot\nabla\eta$. For an ensemble initially in a permutation-symmetric state, after an interval τ_0 with frozen motion in the Zeeman field gradient, the diffraction pattern becomes $I_c = \langle\hat{N}_s\rangle - \frac{P}{N-1} + \frac{P}{N^2-N}|\langle\sum_j e^{-i(\Delta\mathbf{k}-\tau_0\nabla\eta)\cdot\mathbf{r}_j}\rangle|^2$. We focus on situations where $\partial_z\eta$ is either zero or not picked up by atomic ensembles of a quasi-2D geometry in the x-y plane. The in-plane gradient simply results in a displacement of the sharp diffraction peak or dip, preserving its strength and shape (Fig. 3). This has several significant consequences. First, by evolution in an external field of known gradient, entanglement can be detected by measuring the peak or dip along a chosen direction with finite θ, such that the detectors do not pick up laser photons. Second, the displacement measures the vector value of the gradient. It can thus be used as the principle of a vector gradiometer of a magnetic field, a static electric field via the dc Stark effect, and a light field via the ac Stark effect [12].

An ideal probe state is the spin-coherent state of N unentangled atoms with in-plane polarization, which can be realized by optical pumping followed by a spin rotation to the in-plane direction. The gradient is then probed simultaneously by the $\sim N^2$ classical pair correlations, and its vector value is encoded as the displacement of a diffraction peak with strength $\sim N^2$.

Now we analyze the sensitivity of our diffraction-based Zeeman field gradiometer. Consider the atoms in the 1D geometry illustrated in Fig. 4(a) with a Gaussian spatial distribution of full width at half maximum (FWHM) A. Atoms are initialized in the spin-coherent state and evolved in the Zeeman field gradient for an interval of τ_0. The diffraction pattern is then $\frac{N^2}{4}f(\theta) + \frac{N}{4}$, where $f(\theta) \equiv e^{-[(k_0A)^2/4](\theta-\theta_0)^2}$ is a sharp peak centered in a tilted direction: $\theta_0 = k_0^{-1}\tau_0\partial_x\eta$. Our goal is to extract this direction from the photon statistics. The field gradient can then be inferred based on the above relation. The spatial resolution of the gradiometer is just given by the size of the atomic ensemble A. The precision of this measurement is determined by the width of the peak ($\frac{1}{k_0A}$), the shot noise of the photon counts, and the angular resolution ($\delta\theta$) of the CCD detector array. While the CCD angular resolution can always be improved by increasing the distance from the atomic ensemble, the former two factors will determine the quantum limit for the sensitivity of this gradiometer. We will examine the increase of the sensitivity with the number of atoms N used in the probe. Our discussion is limited to the dilute regime (i.e., $k_0A/N \geqslant 2\pi$).

In a single probe using N atoms, the photon counts at each CCD pixel can be written as $n_i + \Delta n_i$, where n_i and Δn_i are respectively the expectation value and the fluctuation of the photon counts. We have

$$n_i = \int_{\theta_i-\delta\theta/2}^{\theta_i+\delta\theta/2} d\theta\left(\frac{N^2}{4}f(\theta) + \frac{N}{4}\right) = \delta\theta\frac{N^2}{4}\bar{f}(\theta_i) + \delta\theta\frac{N}{4}, \tag{9}$$

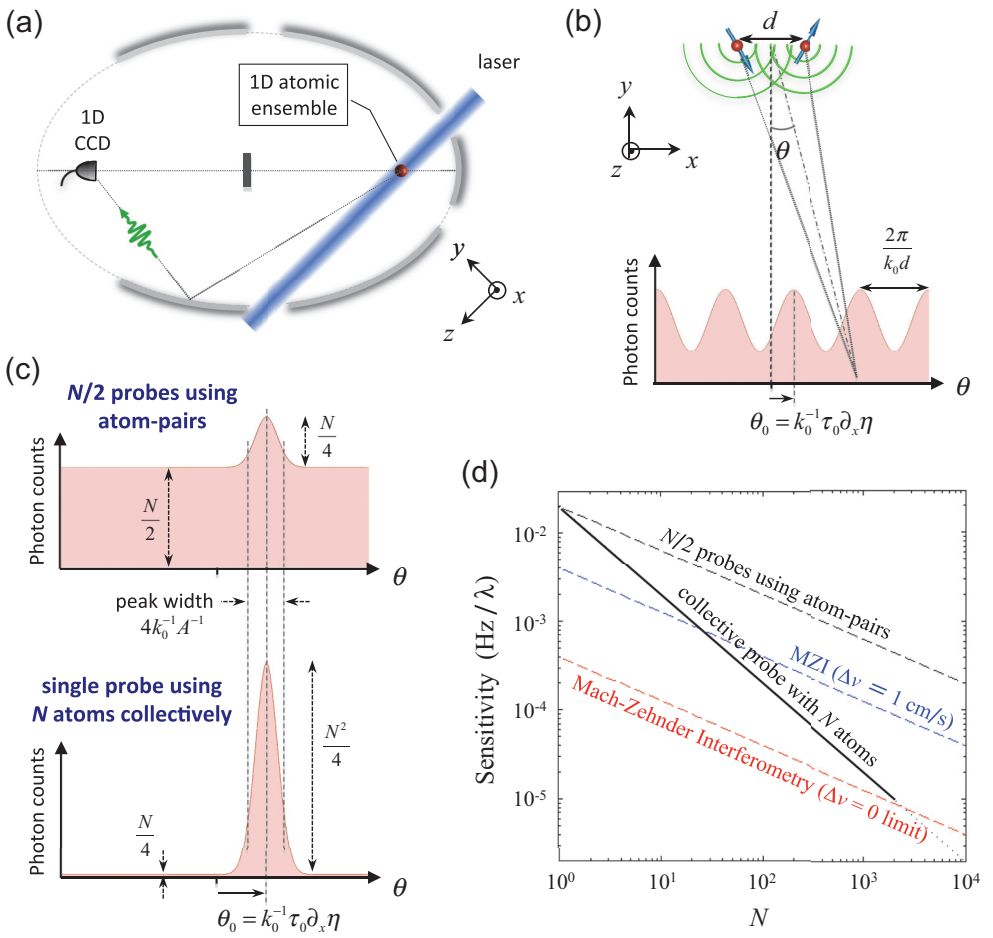

FIG. 4. (Color online) Zeeman field gradiometer using a 1D atomic ensemble. (a),(b) Schematic of the setup. The ensemble and a 1D CCD array are placed respectively on the two common focus lines of a group of elliptical cylinder mirrors. The mirrors ensure that the majority of photons is collected by the detector. The smallest ensemble can be an atom pair, giving a direct analog of double-slit interferometry. (c) Signal of $N/2$ probes using atom pairs (upper panel) and single probe using N atoms collectively (lower panel), with each atom placed randomly on the focus line according to a Gaussian distribution with FWHM A. The peak strength in the lower panel is enhanced by a factor of N. (d) Gradiometer sensitivity at a spatial resolution $A = 1$ mm with a resource of N unentangled atoms. The diffraction-based gradiometer using N atoms collectively ($N/2$ atom pairs independently) has a sensitivity of $1/N$ ($1/\sqrt{N}$) scaling, shown by the solid (dashed) black line. The sensitivity of flying-atom Mach-Zehnder interferometry (MZI) gradiometer is shown for Ref. [38]. The probe time $\tau_0 = A/\Delta v = 0.1$ s for the blue line, limited by a finite velocity uncertainty $\Delta v = 1$ cm/s, while $\tau_0 = 1$ s for all other lines, limited only by the single-spin dephasing time.

where $\bar{f}(\theta_i) \equiv \frac{1}{\delta\theta}\int_{\theta_i-\delta\theta/2}^{\theta_i+\delta\theta/2} d\theta f(\theta)$. Here we assume that the ith pixel of the detector collects all photons emitted within the angle range $[\theta_i - \frac{\delta\theta}{2}, \theta_i + \frac{\delta\theta}{2}]$, where $\theta_i \equiv i\delta\theta$. As shown in Appendix B, the photon statistics is found to be Poissonian when the probe state is a spin-coherent state, and we have

$$\langle \Delta n_i^2 \rangle \sim n_i. \tag{10}$$

From the photon statistics $\{n_i + \Delta n_i\}$, we can extract the peak central position θ_c defined as

$$\theta_c = \frac{\sum_i \theta_i (n_i + \Delta n_i)}{\sum_i (n_i + \Delta n_i)}. \tag{11}$$

θ_c unavoidably has some deviation from θ_0, and the peak-position precision is then defined as $\sqrt{(\theta_c - \theta_0)^2}$. Our analysis shows (see Appendix C) that, when θ_c from a single probe is used to extract the Zeeman field gradient $\partial_x \eta$, the overall precision is

$$\Delta(\partial_x \eta) \sim \frac{k_0}{\tau_0}\sqrt{\frac{4\pi^{-1/2}}{N^2 k_0 A} + (k_0 A)^4 \delta\theta^6}. \tag{12}$$

For small $\delta\theta$, the sensitivity is $\Delta(\partial_x \eta) \sim \frac{k_0}{\tau_0}\frac{1}{N\sqrt{k_0 A}}$ which scales inversely with N.

The smallest ensemble for the gradiometer can just be an atom pair prepared in a spin-coherent state which emits one photon on average in each probe. We can make $N/2$ independent probes using such atom pairs and extract the field gradient from the integrated signal. For one atom at position $\mathbf{x}_1$ and the other atom at $\mathbf{x}_2$, the photon has an emission distribution of $\sim 1 + \frac{1}{2}\cos[\mathbf{k}\cdot(\mathbf{x}_1 - \mathbf{x}_2)]$ see Fig. 4(b). This is a direct analog of double-slit interferometry. We assume that each atom has a fixed position during a single probe but it can randomly appear on a 1D line according to a Gaussian

distribution proportional to e^{-2x^2/A^2} with full width at half maximum A for multiple probes. Summing over $N/2$ probes, the total photon distribution pattern is $\frac{N}{2}+\frac{N}{4}e^{-(k_xA)^2/4}$. The peak strength is thus $\sim N$. Following the previous derivations, we find that the sensitivity for measuring the Zeeman field gradient is $\frac{k_0}{\tau_0}\frac{1}{\sqrt{Nk_0A}}$ with $1/\sqrt{N}$ scaling.

Thus, a single collective probe using N atoms has sensitivity $\sim\frac{1}{N}\frac{k_0}{\tau_0\sqrt{k_0A}}$, which goes beyond the SQL of $\sim\frac{1}{\sqrt{N}}\frac{k_0}{\tau_0\sqrt{k_0A}}$ for $N/2$ independent probes using atom pairs, as shown in Fig. 4(d). The enhancement comes from the N^2 scaling of the peak strength, which is the result of using a large group of atoms collectively. In Fig. 4(d), we also compare with a gradiometer based on a Mach-Zehnder interferometer of flying atoms in an atomic fountain which has the SQL sensitivity of $\sim\frac{1}{\sqrt{N}}\frac{1}{\tau_0A}$, while the inevitable velocity uncertainty further sets a tighter upper bound for τ_0 dependent on the spatial resolution A (see Appendix D).

The collectively enhanced sensitivity with $1/N$ scaling is valid in the dilute regime $N\leqslant k_0A$. Beyond this regime, multiple light scattering cannot be treated perturbatively and its effect will eventually renormalize the peak strength to the N scaling. When atoms are trapped in optical lattices, the probe time τ_0 can be as long as the single-spin homogeneous dephasing time, on the order of 1 s or longer [12]. This diffraction-based gradiometer using stationary atoms is immune to collective noises and uncertainty in atomic positions, and can have a fine spatial resolution (given by the size of the ensemble). Remarkably, for the scheme to work, the probe state does not need to have a high degree of spin polarization as an imperfect polarization p just scales down the sensitivity by $1/p$.

The diffraction image can also be used for a nondemolition probe of atomic motions and temperature in trapped cold atom gases, by introducing a waiting time τ_1 between the imprinting of the phase gradient $\nabla\phi$ on the spin-coherent state and the measurement of the Stokes photon diffraction (Fig. 3). Atomic motions in the interval τ_1 will diminish the spin polarization, resulting in decay of the displaced diffraction peak [11]. For $|\nabla\phi|^2\langle\Delta\mathbf{r}^2\rangle\ll 1$, the peak strength is $\frac{N^2}{4}e^{-|\nabla\phi|^2\langle\Delta\mathbf{r}^2\rangle/3}$, $\langle\Delta\mathbf{r}^2\rangle$ being the mean square displacement of the atoms. For short τ_1 when $\Delta\mathbf{r}$ is small compared to the interatomic distance d, $\langle\Delta\mathbf{r}^2\rangle=2\frac{k_BT}{m}\tau_1^2$. Thus, by preparing a large phase gradient $|\nabla\phi|\sim 1/d$, the short-time motion can be probed and the atomic temperature can be read out from the decay of the peak. A smaller $|\nabla\phi|$ allows the probe of long-time motion which will eventually cross over to the diffusive regime by atomic collisions. τ_1 is upper limited by the spin-dephasing time, which is long enough for observing the entire crossover behavior from ballistic to diffusive motion, providing information about the collisional interactions in trapped gases. The collectively enhanced peak strength of $\sim N^2$ provides sufficient signal-to-noise ratio for determining $\langle\Delta\mathbf{r}^2\rangle$ at a given τ_1 by a single-shot measurement.

VI. SUMMARY

In conclusion, we have shown that the far-field diffraction image of spontaneously emitted Raman photons can be used for detection of spin entanglement in cold atomic ensembles as well as for quantum metrology applications. For many-body states with small or maximum uncertainty in the spin-excitation number, entanglement is witnessed by the presence of either a sharp diffraction peak or a dip. For general states, the relative strength of the peak or dip over its background detects entanglement through the pair-correlation sum rules derived from spin-squeezing inequalities. Spin precessions in a Zeeman field gradient lead to displacement of the diffraction peak or dip while atomic motions lead to decay of its strength. These can serve as principles for a vector gradiometer of fields and for nondemolition measurements of the atomic temperature and collisional dynamics. The gradiometer sensitivity can reach $1/N$ by use of a spin-coherent state of N unentangled atoms as the probe, which suggests a possibility for going beyond the SQL without entanglement. Motional dynamics leads to temporal decay of the diffraction peak which can be used for a nondemolition probe of the temperature and collisional interactions in trapped atomic gases.

ACKNOWLEDGMENTS

The authors thank Lian-ao Wu for helpful discussions. W.Y. thanks CQI at IIIS of Tsinghua for hospitality during his visit through the support by NBRPC under Grant No. 2011CBA00300 (2011CBA00301). The work was supported by the Research Grant Council of Hong Kong under Grants No. HKU706711P and No. HKU8/CRF/11G.

APPENDIX A: PERTURBATIVE SOLUTION TO THE MASTER EQUATION

We assume that the wave vector $\mathbf{k}_0$ of the driving laser is perpendicular to the ensemble (i.e., $\mathbf{k}_0\cdot\mathbf{r}_i=0$). For simplicity of expression, below we replace $\Delta\mathbf{k}\equiv\mathbf{k}-\mathbf{k}_0$ by $\mathbf{k}$ when it appears in $\hat{J}^-(\Delta\mathbf{k})$.

The number of photons collected in a time τ_c along direction $\mathbf{k}$ within the infinitesimal solid angle $\delta\Omega$ is written as $n_p(\mathbf{k},\tau_c)=\Gamma\frac{\delta\Omega}{4\pi}\int_0^{\tau_c}dt\mathrm{Tr}[\hat{J}^+(\mathbf{k})\hat{J}^-(\mathbf{k})\rho(t)]$. Here we have ignored the slowly varying single-atom dipole emission pattern. $\rho(t)$ can be obtained from the master equation [Eq. (7)] by viewing the $\mathcal{L}_1$ term as a perturbation.

We use the notation $\rho^{(n)}(t)$ and $\langle\cdots\rangle_t^{(n)}\equiv\mathrm{Tr}[\cdots\rho^{(n)}(t)]$ to describe the result keeping up to the nth-order effect of $\mathcal{L}_1$. For the zeroth-order result $\rho^{(0)}(t)=e^{\mathcal{L}_0t}\rho(0)$, we have $\langle\hat{\sigma}_m^+\hat{\sigma}_n^-\rangle_t^{(0)}=e^{-\Gamma t}\langle\hat{\sigma}_m^+\hat{\sigma}_n^-\rangle_0$. Then

$$n_p^{(0)}(\mathbf{k},\tau_c)=\frac{\delta\Omega}{4\pi}(1-e^{-\Gamma\tau_c})\langle\hat{J}^+(\mathbf{k})\hat{J}^-(\mathbf{k})\rangle_0. \tag{A1}$$

Below we solve for $\rho^{(1)}(t)$ which captures the leading-order effect of $\mathcal{L}_1$, and show that it is sufficient to account for the effect of $\mathcal{L}_1$ in the dilute limit. We consider an N-atom 1D lattice. In the first-order approximation, the equation of motion for the pair correlation is

$$\begin{aligned}\frac{d\langle\hat{\sigma}_m^+\hat{\sigma}_n^-\rangle_t^{(1)}}{d(\Gamma t)}&=-\langle\hat{\sigma}_m^+\hat{\sigma}_n^-\rangle_t^{(1)}+\sum_{j\neq n}\left(\frac{\Gamma_{jn}}{2\Gamma}-i\frac{G_{jn}}{2\Gamma}\right)\langle\hat{\sigma}_m^+\hat{\sigma}_j^-\hat{\sigma}_n^z\rangle_t^{(0)}\\&\quad+\sum_{j\neq m}\left(\frac{\Gamma_{jm}}{2\Gamma}+i\frac{G_{jm}}{2\Gamma}\right)\langle\hat{\sigma}_m^z\hat{\sigma}_j^+\hat{\sigma}_n^-\rangle_t^{(0)}.\end{aligned} \tag{A2}$$

We denote $\Gamma_j \equiv \Gamma_{n\pm j,n} = \Gamma\frac{\sin|jkd|}{|jkd|}$, $G_j \equiv G_{n\pm j,n} = \Gamma\frac{\cos|jkd|}{|jkd|}$, $a_t^{(0)} \equiv \langle\hat{\sigma}_m^+\hat{\sigma}_m^-\rangle_t^{(0)}$, and $p_t^{(0)} \equiv \langle\hat{\sigma}_m^+\hat{\sigma}_n^-\rangle_{t,m\neq n}^{(0)}$. Then

$$\frac{d\langle\hat{\sigma}_n^+\hat{\sigma}_n^-\rangle_t^{(1)}}{d(\Gamma t)} = -\langle\hat{\sigma}_n^+\hat{\sigma}_n^-\rangle_t^{(1)} - p_t^{(0)}\left(\sum_{j=1}^{N-n}+\sum_{j=1}^{n-1}\right)\frac{\Gamma_j}{\Gamma},$$

$$\begin{aligned}\frac{d\langle\hat{\sigma}_m^+\hat{\sigma}_n^-\rangle_{t,m\neq n}^{(1)}}{d(\Gamma t)} &= -\langle\hat{\sigma}_m^+\hat{\sigma}_n^-\rangle_{t,m\neq n}^{(1)} + 2B_t^{(0)}\frac{\Gamma_{m-n}}{\Gamma}\\ &\quad+\alpha_t^{(0)}\left(\sum_{j=1}^{N-n}+\sum_{j=1}^{n-1}\right)\left(\frac{\Gamma_j}{\Gamma}-i\frac{G_j}{\Gamma}\right)\\ &\quad+\alpha_t^{(0)}\left(\sum_{j=1}^{N-m}+\sum_{j=1}^{m-1}\right)\left(\frac{\Gamma_j}{\Gamma}+i\frac{G_j}{\Gamma}\right),\end{aligned} \tag{A3}$$

where $\alpha_t^{(0)} \equiv \frac{1}{2}\langle\hat{\sigma}_j^+\hat{\sigma}_m^-\hat{\sigma}_n^z\rangle_{t,j\neq m\neq n}^{(0)}$ is the three-body correlation, and $B_t^{(0)} \equiv \frac{1}{2}\langle\hat{\sigma}_m^+\hat{\sigma}_m^-\hat{\sigma}_n^z\rangle_{t,m\neq n}^{(0)} - \alpha_t^{(0)}$.

Using $\langle\hat{J}^+(\mathbf{k})\hat{J}^-(\mathbf{k})\rangle_t^{(1)} = \sum_n\langle\hat{\sigma}_n^+\hat{\sigma}_n^-\rangle_t^{(1)} + \sum_{m\neq n} e^{i\mathbf{k}\cdot(\mathbf{r}_m-\mathbf{r}_n)}\langle\hat{\sigma}_m^+\hat{\sigma}_n^-\rangle_t^{(1)}$ and switching the summation index as

$$\sum_{n=1}^{N}\left(\sum_{j=1}^{N-n}+\sum_{j=1}^{n-1}\right) = \sum_{j=1}^{N-1}\left(\sum_{n=1}^{N-j}+\sum_{n=j+1}^{N}\right), \tag{A4}$$

we write

$$\begin{aligned}&\frac{d\langle\hat{J}^+(\mathbf{k})\hat{J}^-(\mathbf{k})\rangle_t^{(1)}}{d(\Gamma t)}\\ &= -\langle\hat{J}^+(\mathbf{k})\hat{J}^-(\mathbf{k})\rangle_t^{(1)} + 4(N-j)\\ &\quad\times\sum_{j=1}^{N-1}\frac{\Gamma_j}{\Gamma}\left[B_t^{(0)}\cos(j\mathbf{k}\cdot\mathbf{d}) - \frac{1}{2}p_t^{(0)} - \alpha_t^{(0)}\right]\\ &\quad+\alpha_t^{(0)}\left[\sum_{j=1}^{N-1}\left(\frac{\Gamma_j}{\Gamma}-i\frac{G_j}{\Gamma}\right)f_j(\mathbf{k}) + \text{c.c.}\right],\end{aligned} \tag{A5}$$

where $\mathbf{d}$ is the vector connecting neighboring atoms, and

$$\begin{aligned}f_j(\mathbf{k}) &\equiv \left(\sum_{m=1}^{N}e^{i\mathbf{k}\cdot\mathbf{r}_m}\right)\left(\sum_{n=1}^{N-j}+\sum_{n=j+1}^{N}\right)e^{-i\mathbf{k}\cdot\mathbf{r}_n}\\ &= 2\cos^2\left(\frac{j\mathbf{k}\cdot\mathbf{d}}{2}\right)\frac{\sin^2\left(\frac{N\mathbf{k}\cdot\mathbf{d}}{2}\right)}{\sin^2\left(\frac{\mathbf{k}\cdot\mathbf{d}}{2}\right)}\\ &\quad-\frac{\sin(N\mathbf{k}\cdot\mathbf{d})\sin(j\mathbf{k}\cdot\mathbf{d})}{2\sin^2\left(\frac{\mathbf{k}\cdot\mathbf{d}}{2}\right)}.\end{aligned} \tag{A6}$$

As $\Gamma_j, G_j \sim \frac{1}{jkd}$, only those j terms with $j \ll N$ make significant contributions. Thus $\frac{\sin(N\mathbf{k}\cdot\mathbf{d})\sin(j\mathbf{k}\cdot\mathbf{d})}{2\sin^2(\frac{\mathbf{k}\cdot\mathbf{d}}{2})}$ can be ignored compared to $\cos^2(\frac{j\mathbf{k}\cdot\mathbf{d}}{2})\frac{\sin^2(\frac{N\mathbf{k}\cdot\mathbf{d}}{2})}{\sin^2(\frac{\mathbf{k}\cdot\mathbf{d}}{2})}$. Then

$$\begin{aligned}&\frac{d\langle\hat{J}^+(\mathbf{k})\hat{J}^-(\mathbf{k})\rangle_t^{(1)}}{d(\Gamma t)}\\ &\approx -\langle\hat{J}^+(\mathbf{k})\hat{J}^-(\mathbf{k})\rangle_t^{(1)} + \frac{2\alpha_t^{(0)}}{p_t^{(0)}}\sum_{j>0}\frac{\Gamma_j}{\Gamma}[\cos(j\mathbf{k}\cdot\mathbf{d})+1]\\ &\quad\times\langle\hat{J}^+(\mathbf{k})\hat{J}^-(\mathbf{k})\rangle_t^{(0)} + N\sum_{j>0}\frac{\Gamma_j}{\Gamma}[C_2\cos(j\mathbf{k}\cdot\mathbf{d})+C_3],\end{aligned} \tag{A7}$$

with $C_2 \equiv 4B_t^{(0)} - 2\alpha_t^{(0)}(\frac{a_t^{(0)}}{p_t^{(0)}}-1)$ and $C_3 \equiv -2p_t^{(0)} - 2\alpha_t^{(0)}(\frac{a_t^{(0)}}{p_t^{(0)}}+1)$. In the above equation we have used the relation $\langle\hat{J}^+(\mathbf{k})\hat{J}^-(\mathbf{k})\rangle_t^{(0)} = N(a_t^{(0)} - p_t^{(0)}) + p_t^{(0)}\frac{\sin^2(\frac{N\mathbf{k}\cdot\mathbf{d}}{2})}{\sin^2(\frac{\mathbf{k}\cdot\mathbf{d}}{2})}$.

The time dependences of $a_t^{(0)}$, $p_t^{(0)}$, $\alpha_t^{(0)}$, and $B_t^{(0)}$ are easily obtained from $\rho^{(0)}(t)$:

$$\begin{aligned}a_t^{(0)} &= e^{-\Gamma t}a_0^{(0)}, \quad p_t^{(0)} = e^{-\Gamma t}p_0^{(0)},\\ \alpha_t^{(0)} &= e^{-2\Gamma t}\alpha_0^{(0)} - \tfrac{1}{2}e^{-\Gamma t}(1-e^{-\Gamma t})p_0^{(0)},\\ B_t^{(0)} &= \tfrac{1}{4}e^{-2\Gamma t}\langle(\hat{\sigma}_m^z+1)(\hat{\sigma}_n^z+1)\rangle_0 - \tfrac{1}{2}e^{-\Gamma t}a_0^{(0)} - \alpha_t^{(0)}.\end{aligned} \tag{A8}$$

Solving the differential equation (A7), we obtain the photon-diffraction pattern under the first-order approximation:

$$\begin{aligned}&n_p^{(1)}(\mathbf{k},\tau_c)\\ &= \Gamma\frac{\delta\Omega}{4\pi}\int_0^{\tau_c}dt\,\langle\hat{J}^+(\mathbf{k})\hat{J}^-(\mathbf{k})\rangle_t\\ &\approx \frac{\delta\Omega}{4\pi}N\sum_{j>0}\frac{\Gamma_j}{\Gamma}[f_2(\tau_c)\cos(j\mathbf{k}\cdot\mathbf{d}) + f_3(\tau_c)]\\ &\quad+\frac{\delta\Omega}{4\pi}\left[1-e^{-\Gamma\tau_c}+f_1(\tau_c)\sum_{j>0}\frac{\Gamma_j}{\Gamma}[\cos(j\mathbf{k}\cdot\mathbf{d})+1]\right]\\ &\quad\times\langle\hat{J}^+(\mathbf{k})\hat{J}^-(\mathbf{k})\rangle_0,\end{aligned} \tag{A9}$$

where

$$\begin{aligned}f_1(\tau_c) &= (1-e^{-\Gamma\tau_c})^2\frac{\alpha_0^{(0)}}{p_0^{(0)}} + \Gamma\tau_c e^{-\Gamma\tau_c} + \frac{1}{2}e^{-2\Gamma\tau_c} - \frac{1}{2},\\ f_2(\tau_c) &= \frac{1}{2}(1-e^{-\Gamma\tau_c})^2\langle(\hat{\sigma}_m^z+1)(\hat{\sigma}_n^z+1)\rangle_0\\ &\quad+(1-\Gamma\tau_c e^{-\Gamma\tau_c}-e^{-\Gamma\tau_c})(p_0^{(0)}-a_0^{(0)})\\ &\quad-(1-e^{-\Gamma\tau_c})^2\left(\frac{\alpha_0^{(0)}}{p_0^{(0)}}+\frac{1}{2}\right)(a_0^{(0)}+p_0^{(0)}),\\ f_3(\tau_c) &= -(1-e^{-\Gamma\tau_c})^2\left(\frac{\alpha_0^{(0)}}{p_0^{(0)}}+\frac{1}{2}\right)(a_0^{(0)}+p_0^{(0)})\\ &\quad+(1-\Gamma\tau_c e^{-\Gamma\tau_c}-e^{-\Gamma\tau_c})(a_0^{(0)}-p_0^{(0)}).\end{aligned} \tag{A10}$$

$f_1(\tau_c), f_2(\tau_c), f_3(\tau_c) \sim O((\Gamma\tau_c)^2)$ for $\Gamma\tau_c \ll 1$.

Comparing Eqs. (A1) and (A9), we can see that the modulation of the diffraction pattern by multiple light scattering is described by $\cos(j\mathbf{k}\cdot\mathbf{d})$. The dipole-dipole interaction with coefficients G_j has a vanishing first-order effect, and thus it does not appear in our derivation above. Obviously for $j \ll N$ the modulation is slowly varying in $\mathbf{k}$ space. We are interested only in the diffraction pattern in the neighborhood of the forward direction where $\cos(j\mathbf{k}\cdot\mathbf{d}) \approx 1$; then $n_p^{(1)}(\tau_c\to\infty) = \beta_1 n_p^{(0)}(\tau_c\to\infty) + \frac{\delta\Omega}{4\pi}N\beta_2$, with $\beta_1 = 1 + 2f_1(\tau_c\to\infty)\sum_{j>0}\frac{\Gamma_j}{\Gamma}$ and $\beta_2 = [f_2(\tau_c\to\infty) + f_3(\tau_c\to\infty)]\sum_{j>0}\frac{\Gamma_j}{\Gamma}$. The peak- or dip-to-background ratio of the initial diffraction pattern (i.e., as $\tau_c \to 0$) is $r^{(0)} = \frac{N^2p_0^{(0)}}{N[a_0^{(0)}-p_0^{(0)}]}$,

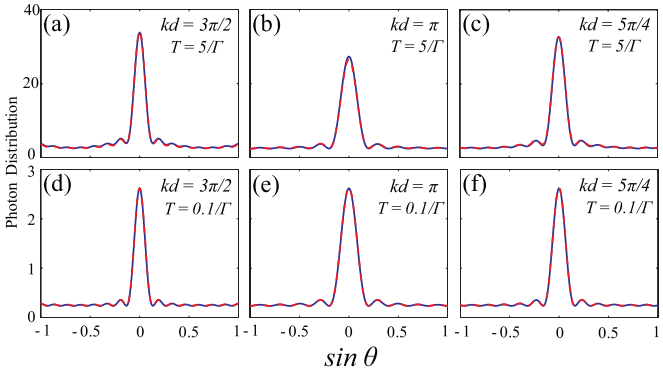

FIG. 5. (Color online) Diffraction pattern of Stokes photons emitted by a chain of ten atoms initially in the spin-coherent state with in-plane polarization $\otimes_{j=1}^{10}\frac{|\uparrow\rangle_j+|\downarrow\rangle_j}{\sqrt{2}}$. With the collection interval $T = 5/\Gamma$, 99.3% of all spin excitations are converted into Stokes photons, and with $T = 0.1/\Gamma$, 10% of all spin excitations are converted into Stokes photons. Red dashed lines: exact numerical solution of the master equation Eq. (7). Blue solid lines in (a)–(c): perturbative solution keeping the first-order effect of $\mathcal{L}_1$ [i.e., Eq. (A9)]. Blue solid lines in (d)–(f): the zeroth-order solution without $\mathcal{L}_1$ [i.e., Eq. (A1)].

which measures the pair-correlation sum of the initial atomic state of interest. In the diffraction pattern of all emitted photons (i.e., as $\tau_c \to \infty$), it becomes

$$r^{(1)} = \frac{\beta_1 N^2 p_0^{(0)} + N\beta_2}{\beta_1 N\left[a_0^{(0)} - p_0^{(0)}\right] + N\beta_2} = (1+\delta)r^{(0)},$$
$$\delta \cong \frac{\beta_2}{\beta_1\left[a_0^{(0)} - p_0^{(0)}\right] + \beta_2}. \tag{A11}$$

Since $\sum_{j>0}\frac{\Gamma_j}{\Gamma} \approx \frac{1}{kd}\int_0^\infty \frac{\sin x}{x}dx \sim \frac{1}{kd} \ll 1$, we expect $\beta_1 \approx 1$ and $\beta_2 \ll 1$. Thus $\delta \ll 1$. When the initial atomic state is an eigenstate of $\hat{J}_z$ or a separable state, we have

$$\delta \cong \frac{-2a_0^{(0)}p_0^{(0)}\sum_{j>0}\frac{\Gamma_j}{\Gamma}}{a_0^{(0)} - p_0^{(0)}}. \tag{A12}$$

We note that $p_0^{(0)} = P/(N^2 - N)$, which has the maximum value of $1/4$ in the neighborhood of a Dicke state with half-spin

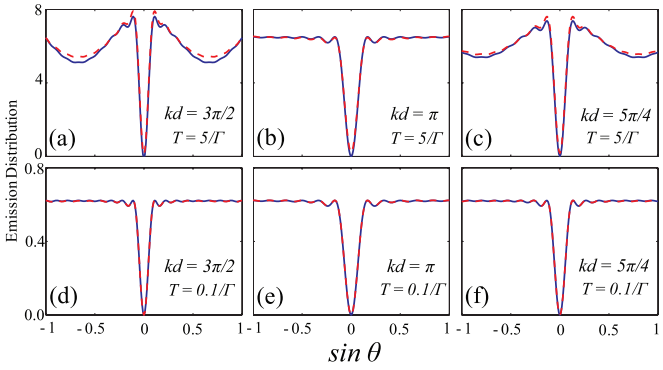

FIG. 6. (Color online) Diffraction pattern of Stokes photons emitted by a chain of 12 atoms initially in a many-body singlet state (i.e., $J = 0$, $M = 0$). Red dashed lines: exact numerical solution of the master equation (7). Blue solid lines in (a)–(c): perturbative solution keeping the first-order effect of $\mathcal{L}_1$ [i.e., Eq. (A9)]. Blue solid lines in (d)–(f): the zeroth-order solution without $\mathcal{L}_1$ [i.e., Eq. (A1)].

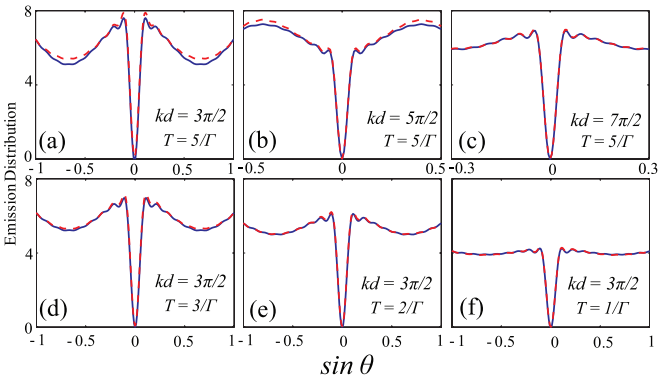

FIG. 7. (Color online) Diffraction pattern of Stokes photons emitted by a chain of 12 atoms initially in the many-body singlet state (i.e., $J = 0$, $M = 0$) with various lengths of the collection time T. Red dashed lines: exact numerical solution of the master equation (7). Blue solid lines: perturbative solution keeping the first-order effect of $\mathcal{L}_1$ [i.e., Eq. (A9)].

excitation. For typical states, $p_0^{(0)} \sim 1/N$ and then δ scales inversely with N.

To examine the convergence of the perturbation solution, we compare it with the exact numerical solution of the master equation for a small ensemble in a 1D lattice with various lattice constants d. The magnitude of the multiple-light-scattering terms in $\mathcal{L}_1$ decays fast with the distance; thus only the nearest-neighbor terms are important. Because of the limits of our computation capability, in the calculation presented in Figs. 5–7 when referring to multiple light scattering, we keep only the nearest-neighbor terms in $\mathcal{L}_1$ (i.e., those with coefficients Γ_1) and artificially set $\Gamma_j = 0$ for $j \geqslant 2$. But for the dipole-dipole interaction all G_j terms are considered in the exact numerical solution. For this reduced master equation, we compare the perturbative and the exact numerical solutions. We can see that the perturbative solution keeping the first-order effect of $\mathcal{L}_1$ [i.e., Eq. (A9)] has excellent convergence to the exact numerical solution for both the dip and peak patterns. In particular, the multiple light scattering has negligible effects if we set the collection time $T \leqslant 0.1/\Gamma$. Note that in the initial interval of $T = 0.1/\Gamma$, 10% of all spin zexcitations are already converted into Stokes photons. In Fig. 8, we

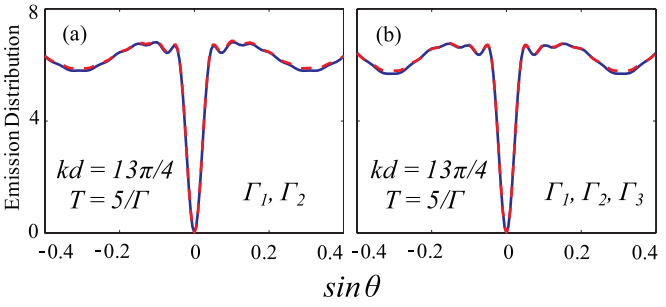

FIG. 8. (Color online) The results including not only the nearest-neighbor Γ_1 term, but also (a) the next-nearest-neighbor Γ_2 and (b) the Γ_2 and Γ_3 terms for a 12-qubit $J = 0$, $M = 0$ permutation-invariant state. Values of d and T are given in the figure. Red dashed lines: the numerical simulated results. Blue solid lines: the fitting using Eq. (A9). The dipole-dipole interaction G_j is not considered here.

show that the effects of next-nearest-neighbor terms in $\mathcal{L}_1$ (i.e., with coefficients Γ_2 and Γ_3) are also well accounted for by the perturbative solutions in Eq. (A9). This calculation also confirms that the modulation of the diffraction pattern is dominated by the near-neighbor cross terms, and the effect of the Γ_3 term is already small as compared to the Γ_1 and Γ_2 terms.

We have also considered a 2D atomic ensemble in the xy plane in a large trap, where the atomic number density is Gaussian $n(\mathbf{r}) = n(0)e^{-2r^2/A^2}$ at position $\mathbf{r}$ with A the full width at half maximum. The total atom number is given by $N = \int d\mathbf{r} n(\mathbf{r}) = \frac{\pi}{2} n(0) A^2$ with the dilute condition $k_0 A\sqrt{N} \geqslant 2\pi$ satisfied. The result is similar to the case of a 1D lattice in that the peak- or dip-to-background ratio is only slightly changed.

For a dilute hot atomic vapor where atomic motion is much faster than the Stokes photon emission, we find that the diffraction pattern is similar to that of cold atoms in the neighborhood of the forward direction, i.e., with a sharp diffraction peak or dip from which the pair-correlation sum of atoms can be read out. Since atoms move around on a time scale faster than the photon emission, the coefficients of the cross terms in $\mathcal{L}_1$ should be replaced by $\Gamma_{jj'} = \Gamma\langle \frac{\sin(k_0|\mathbf{r}_j - \mathbf{r}_{j'}|)}{k_0|\mathbf{r}_j - \mathbf{r}_{j'}|}\rangle_{\text{mot}} = \frac{\Gamma}{2(k_0A)^2}$ and $G_{jj'} = \frac{G}{(k_0A)^2}$, which are independent of j and j' [20]. Here A is the size of the atomic vapor. The original master equation (7) becomes

$$\begin{aligned}\dot{\rho} = {} & \frac{\Gamma}{2}\sum_j (2\hat{\sigma}_j^- \rho \hat{\sigma}_j^+ - \hat{\sigma}_j^+\hat{\sigma}_j^-\rho - \rho\hat{\sigma}_j^+\hat{\sigma}_j^-) \\ & + \frac{\Gamma}{4(k_0A)^2}(2\hat{J}^-\rho\hat{J}^+ - \hat{J}^+\hat{J}^-\rho - \rho\hat{J}^+\hat{J}^-) \\ & + i\frac{G}{2(k_0A)^2}\left[\hat{J}_x^2 + \hat{J}_y^2, \rho\right]. \end{aligned} \tag{A13}$$

In the right-hand side (RHS) of the above master equation, the first term corresponds to atoms independently emitting photons, the second term comes from multiple light scattering, and the third term is the dipole-dipole interaction. Then

$$\begin{aligned}\frac{d\langle \hat{J}_z\rangle_t}{dt} &= -\Gamma\left(\frac{N}{2} + \langle \hat{J}_z\rangle_t\right) - \frac{\Gamma}{2(k_0A)^2}\langle \hat{J}^+\hat{J}^-\rangle_t, \\ \frac{d\langle \hat{J}^+\hat{J}^-\rangle_t}{dt} &= -\Gamma\langle \hat{J}^+\hat{J}^-\rangle_t + \frac{\Gamma}{(k_0A)^2}\langle \hat{J}^+\hat{J}_z\hat{J}^-\rangle_t. \end{aligned} \tag{A14}$$

The angular distribution of the emission rate is given by

$$\begin{aligned}\langle \hat{J}^+(\mathbf{k})\hat{J}^-(\mathbf{k})\rangle_t = {} & \frac{N}{2} + \langle \hat{J}_z\rangle_t + \left(\langle \hat{J}^+\hat{J}^-\rangle_t - \langle \hat{J}_z\rangle_t - \frac{N}{2}\right) \\ & \times |\langle e^{i\Delta\mathbf{k}\cdot\mathbf{r}_j}\rangle_{\text{mot}}|^2. \end{aligned} \tag{A15}$$

Just as in the case of a dilute cold atom ensemble, the initial diffraction pattern has a sharp diffraction peak or dip in the forward direction with a width given by $\frac{1}{k_0A}$ and a strength determined by the pair-correlation sum $P = \langle \hat{J}^+\hat{J}^-\rangle_0 - \langle \hat{J}_z\rangle_0 - \frac{N}{2}$. The value of the pair-correlation sum can be read out from the ratio of the peak or dip to the neighboring background. From Eq. (A14), we can see that the background part $\frac{N}{2} + \langle \hat{J}_z\rangle_t$ in the emission rate decays with time, and the existence of the $\frac{\Gamma}{2(k_0A)^2}\langle \hat{J}^+\hat{J}^-\rangle_t$ term makes the decay faster. On the other hand, the peak or dip strength $\langle \hat{J}^+\hat{J}^-\rangle_t - \langle \hat{J}_z\rangle_t - \frac{N}{2}$ may increase with time as long as $\frac{\langle \hat{J}^+\hat{J}_z\hat{J}^-\rangle_t}{(k_0A)^2} + \frac{\langle \hat{J}^+\hat{J}^-\rangle_t}{2(k_0A)^2} > \langle \hat{J}^+\hat{J}^-\rangle_t - \langle \hat{J}_z\rangle_t - \frac{N}{2}$. This is just the case discussed in the study of super-radiance phenomena by Rehler and Eberly [14], where the authors show that in a very dense ensemble a directional super-radiance may develop at a later time even when the initial state's emission pattern is almost isotropic in all directions and has no super-radiance behavior.

Here we are interested in how the peak- or dip-to-background ratio evolves as a function of the collection interval. It is obvious that only the second terms in the RHS of both equations in Eq. (A14) can change this ratio. When the dilute condition $(k_0A)^2/N \geqslant (2\pi)^2$ is satisfied, $\frac{\langle \hat{J}^+\hat{J}^-\rangle_t}{2(k_0A)^2} \ll \frac{N}{2} + \langle \hat{J}_z\rangle_t$ and $\frac{\langle \hat{J}^+\hat{J}_z\hat{J}^-\rangle_t}{(k_0A)^2} \ll \langle \hat{J}^+\hat{J}^-\rangle_t$, and the effect is negligible as compared to the first terms. Thus, the peak- or dip-to-background ratio is barely changed by multiple light scattering and the dipole-dipole interaction when the dilute condition is satisfied.

APPENDIX B: PHOTON-NUMBER FLUCTUATIONS

We analyze the shot noise of the photon counts at the detectors. The total number of Stokes photons in a given direction $\mathbf{k}$ at collection time τ_c is given by $n_p(\tau_c) = \sum_{\mathbf{k}}\langle \hat{a}_{\mathbf{k}}^\dagger(\tau_c)\hat{a}_{\mathbf{k}}(\tau_c)\rangle$; here the summation is over a finite solid angle $\delta\Omega$. From the effective light-atom coupling Hamiltonian [Eq. (1)], the evolution of the photon operator is

$$\hat{a}_{\mathbf{k}}(t) = \hat{a}_{\mathbf{k}}(0)e^{-i\omega_k t} + ig_{\mathbf{k}}\int_0^t d\tau\, \hat{J}^-(\mathbf{k},\tau)e^{-i\omega_{\mathbf{k}}(t-\tau)}. \tag{B1}$$

The photon-number fluctuation can then be expressed in terms of the atomic correlations:

$$\begin{aligned}\Delta n_p^2 &\equiv \left\langle\left(\sum_{\mathbf{k}}\hat{a}_{\mathbf{k}}^\dagger(\tau_c)\hat{a}_{\mathbf{k}}(\tau_c)\right)^2\right\rangle - \left\langle\sum_{\mathbf{k}}\hat{a}_{\mathbf{k}}^\dagger(\tau_c)\hat{a}_{\mathbf{k}}(\tau_c)\right\rangle^2 \\ &= n_p - n_p^2 + \sum_{\mathbf{k}\mathbf{k}'}\langle \hat{a}_{\mathbf{k}}^\dagger(\tau_c)\hat{a}_{\mathbf{k}'}^\dagger(\tau_c)\hat{a}_{\mathbf{k}}(\tau_c)\hat{a}_{\mathbf{k}'}(\tau_c)\rangle \\ &= n_p - n_p^2 + \frac{2}{(4\pi)^2}\int d\Omega_{\mathbf{k}} d\Omega_{\mathbf{k}'}\int_0^{\tau_c} dt_1\int_0^{t_1} dt_2 \\ &\quad \times \langle \hat{J}^+(\mathbf{k}',t_2)\hat{J}^+(\mathbf{k},t_1)\hat{J}^-(\mathbf{k},t_1)\hat{J}^-(\mathbf{k}',t_2)\rangle. \end{aligned} \tag{B2}$$

Here for simplicity we have ignored the slowly varying single-atom dipole emission pattern.

In Appendix A, we have shown that the $\mathcal{L}_1$ term in the master equation results in only a small modulation on the diffraction pattern. Thus, in deriving Δn_p^2 the effect of the $\mathcal{L}_1$ term will not be considered since we are interested only in the order of magnitude of the fluctuation. From the quantum regression theorem [39], we have $\langle \hat{J}^+(\mathbf{k}',t)\hat{J}^+(\mathbf{k},t+\tau)\hat{J}^-(\mathbf{k},t+\tau)\hat{J}^-(\mathbf{k}',t)\rangle = e^{-\Gamma\tau-2\Gamma t}\text{Tr}[\hat{J}^+(\mathbf{k}')\hat{J}^+(\mathbf{k})\hat{J}^-(\mathbf{k})\hat{J}^-(\mathbf{k}')\rho(0)]$, assuming that a CCD pixel collects photons emitted in a small solid angle $\delta\Omega \lesssim \frac{1}{N}$. During the time interval of 0 to ∞, we find the expectation value and fluctuation in the number of photons

collected by a pixel placed in the direction of $\mathbf{k}$:

$$n_p \approx \frac{\delta\Omega}{4\pi}\mathrm{Tr}[\hat{J}^+(\mathbf{k})\hat{J}^-(\mathbf{k})\rho(0)],$$
$$\Delta n_p^2 \approx \frac{\delta\Omega^2}{(4\pi)^2}\mathrm{Tr}[\hat{J}^+(\mathbf{k})\hat{J}^+(\mathbf{k})\hat{J}^-(\mathbf{k})\hat{J}^-(\mathbf{k})\rho(0)] + n_p - n_p^2. \tag{B3}$$

For an atomic ensemble initially in eigenstates of $\hat{J}_z$ or spin-coherent states with in-plane polarization, a straightforward calculation shows that $n_p \sim N^2\delta\Omega \sim N$ and $\Delta n_p^2 \sim n_p$ for $\mathbf{k}$ in the neighborhood of the forward direction, and $n_p \sim N\delta\Omega \sim 1$ and $\Delta n_p^2 \sim n_p$ for $\mathbf{k}$ away from the forward direction, i.e., the photon statistics is Poissonian.

APPENDIX C: EXTRACTION OF THE PEAK POSITION FROM THE PHOTON STATISTICS

The most intuitive way to define the central position from the photon distribution $\{n_i + \Delta n_i\}$ collected at the CCD pixels is

$$\theta_c = \frac{\sum_i \theta_i(n_i + \Delta n_i)}{\sum_i (n_i + \Delta n_i)} = \bar{\theta}_c + \frac{\sum_i(\theta_i - \bar{\theta}_c)\Delta n_i}{\sum_i (n_i + \Delta n_i)}, \tag{C1}$$

where θ_c is the peak central position extracted from a single probe, and $\bar{\theta}_c \equiv \frac{\sum_i \theta_i n_i}{\sum_i n_i}$ is the expectation value of θ_c in an ensemble measurement consisting of many probes. We first show that $\bar{\theta}_c$ can infinitely approach θ_0 with sufficient resolution of the CCD.

For large N, we can neglect the homogeneous background which is smaller than the peak feature by a factor of N, and write

$$\bar{\theta}_c = \frac{\sum_i \theta_i \bar{f}(\theta_i)}{\sum_i \bar{f}(\theta_i)} = \frac{\int_{\theta_{\min}}^{\theta_{\max}} d\theta\theta f(\theta)}{\int_{\theta_{\min}}^{\theta_{\max}} d\theta f(\theta)} + \epsilon = \theta_0 + \epsilon. \tag{C2}$$

The deviation ϵ comes from transforming the summation into an integral, which is written

$$\begin{aligned}\epsilon &= \frac{\sum_i \int_{\theta_i-\delta\theta/2}^{\theta_i+\delta\theta/2} d\theta(\theta_i - \theta) f(\theta)}{\int_{\theta_{\min}}^{\theta_{\max}} d\theta f(\theta)} \\ &= \frac{\sum_i \int_0^{\delta\theta/2} d\theta\theta[f(\theta_i + \theta) - f(\theta_i - \theta)]}{\int_{\theta_{\min}}^{\theta_{\max}} d\theta f(\theta)} \\ &\approx \frac{2\int_0^{\delta\theta/2} d\theta\theta^2 \sum_i \frac{df(\theta)}{d\theta}|_{\theta=\theta_i}}{\int_{\theta_{\min}}^{\theta_{\max}} d\theta f(\theta)}.\end{aligned} \tag{C3}$$

Because the function $f(\theta)$ satisfies $\frac{df(\theta_0+\theta)}{d\theta} = -\frac{df(\theta_0-\theta)}{d\theta}$, for every pixel index i we can find j such that $\theta_i - \theta_0 = \theta_0 - \theta_j + O(\delta\theta)$, so $\frac{df(\theta)}{d\theta}|_{\theta=\theta_i} + \frac{df(\theta)}{d\theta}|_{\theta=\theta_j} \sim (k_0A)^2 f(\theta_i)\delta\theta + O(\delta\theta^2)$. Thus the deviation in Eq. (C3) becomes

$$\epsilon \sim (k_0A)^2 \int_0^{\delta\theta/2} d\theta\theta^2 \sim (k_0A)^2\delta\theta^3, \tag{C4}$$

which is $O(\delta\theta^3)$. When $\delta\theta \geqslant \frac{1}{k_0A}$, the sensitivity is determined by the CCD resolution. When $\delta\theta \ll \frac{1}{k_0A}$, $\bar{\theta}_c$ can infinitely approach θ_0.

In a single probe, the sensitivity is limited by the photon shot noise, which leads to uncertainty of θ_c:

$$\begin{aligned}\sqrt{(\theta_c - \bar{\theta}_c)^2} &\approx \frac{\sqrt{\sum_i(\theta_i - \bar{\theta}_c)^2\Delta n_i^2}}{\sum_i n_i} \\ &\approx \frac{2}{N\sqrt{k_0A}} \frac{\sqrt{\int dx x^2 e^{-x^2/4}}}{\int dx e^{-x^2/4}} \\ &= \frac{2\pi^{-1/4}}{N\sqrt{k_0A}}.\end{aligned} \tag{C5}$$

Thus, in using Eq. (C1) to extract the Zeeman field gradient $\partial_x\eta$ from a single probe, the overall precision is

$$\Delta(\partial_x\eta) \sim \frac{k_0}{\tau_0}\sqrt{\frac{4\pi^{-1/2}}{N^2k_0A} + (k_0A)^4\delta\theta^6}. \tag{C6}$$

For small $\delta\theta$, the sensitivity is $\Delta(\partial_x\eta) \sim \frac{k_0}{\tau_0}\frac{1}{N\sqrt{k_0A}}$ which scales inversely with N.

We can also use a function $g(\theta_i,\alpha) = \delta\theta\frac{N^2}{4}e^{-[(k_0A)^2/4](\theta_i-\alpha)^2} + \delta\theta\frac{N}{4}$ to fit the obtained data $n_i + \Delta n_i$. The peak position θ_c is defined as the value of α which minimizes $\sum_i[g(\theta_i,\alpha) - n_i - \Delta n_i]^2$. This method gives the same sensitivity $\Delta(\partial_x\eta) \sim \frac{k_0}{\tau_0}\frac{1}{N\sqrt{k_0A}}$ for small $\delta\theta$.

APPENDIX D: GRADIOMETER USING FLYING-ATOM MACH-ZEHNDER INTERFEROMETRY

The standard method for a field gradiometer is based on phase estimation using a flying-atom Mach-Zehnder interferometer [38,40] (see Fig. 9). First, a $\pi/2$ pulse is applied to prepare an atom in a superposition of spin-up and spin-down states, which is then launched from $x = 0$ with a velocity v. After free evolution for an interval $\tau_0/2$, a π pulse is applied to flip the spin. Finally, another $\pi/2$ pulse is applied and the population on the spin-up state is measured to observe the interference signal. In the first interval of $\tau_0/2$, the spin-up and -down states acquire a relative phase shift $\phi_1 = (\eta_0 + \frac{v\tau_0\partial_x\eta}{4})\frac{\tau_0}{2}$, where η_0 is the homogeneous part of the Zeeman field and $\partial_x\eta$ is the gradient to be measured. $v\tau_0/2 = A/2$ is the distance traveled by the atom with velocity v. In the second interval of $\tau_0/2$, the Zeeman field induces a phase shift $\phi_2 = -(\eta_0 + \frac{3v\tau_0\partial_x\eta}{4})\frac{\tau_0}{2}$. By measuring the population of the spin-up state, this MZI gives an estimate of the total phase $\phi \equiv \phi_1 + \phi_2 = -\frac{1}{4}v\tau_0^2\partial_x\eta$ from which the gradient is then inferred: $\partial_x\eta = -\frac{4\phi}{v\tau_0^2}$.

The sensitivity of the gradiometer is limited by the shot noise $\Delta\phi$ for phase estimation, and the uncertainty in velocity

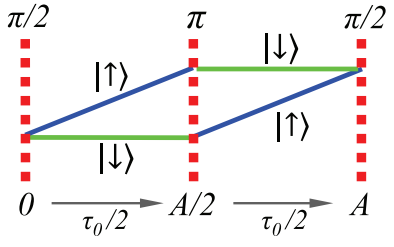

FIG. 9. (Color online) Gradiometer based on flying-atom Mach-Zehnder interferometry.

Δv. In the ith probe using a single atom, the phase one readout can be written as

$$\phi_i = \tfrac{1}{4}\partial_x \eta \tau_0^2 (\bar{v} + \Delta v_i) + \Delta\phi_i, \tag{D1}$$

where $\Delta\phi_i$ is the error in the phase estimation. $\bar{v}$ and Δv_i are respectively the expectation value and uncertainty in velocity. The inferred value of the gradient is then

$$\partial_x \eta^{(i)} \equiv \frac{4\phi_i}{\tau_0^2 \bar{v}} = \partial_x \eta + \partial_x \eta \frac{\Delta v_i}{\bar{v}} + \frac{4\Delta\phi_i}{\tau_0^2 \bar{v}}. \tag{D2}$$

Using an ensemble of N atoms, the error in measuring the gradient is

$$\frac{1}{N}\sqrt{\sum_i (\partial_x \eta^{(i)} - \partial_x \eta)^2} = \frac{\partial_x \eta}{\bar{v}} \frac{1}{\sqrt{N}} \sqrt{\frac{1}{N}\sum_i \Delta v_i^2} + \frac{4}{\tau_0^2 \bar{v}} \frac{1}{\sqrt{N}} \sqrt{\frac{1}{N}\sum_i \Delta\phi_i^2}. \tag{D3}$$

$\sqrt{\frac{1}{N}\sum_i \Delta\phi_i^2} = 1$ which is the shot noise for phase estimation using the MZI [3]. Thus the precision of the MZI scheme is

$$\Delta(\partial_x \eta) = \partial_x \eta \frac{\Delta v}{\sqrt{N}\bar{v}} + \frac{4}{\sqrt{N}\tau_0 A}, \tag{D4}$$

where $A = \bar{v}\tau_0$ represents the spatial resolution of the gradiometer and $\Delta v = \sqrt{\frac{1}{N}\sum_i \Delta v_i^2}$ is the velocity uncertainty.

For atoms launched by an atomic fountain, the uncertainty in atom velocity is intrinsically limited by the temperature: $\Delta v \sim \sqrt{k_B T/m}$. For example, with a temperature of $T \sim 1\ \mu$K, $\Delta v \sim 1$ cm/s. To reduce the error caused by this velocity uncertainty [the first term on the RHS of Eq. (D4)], $\bar{v}$ will be large as compared to Δv. This then sets an upper bound for the probe time at a desired spatial resolution since $\tau_0 = A/\bar{v}$.

[1] I. Bloch, J. Dalibard, and W. Zwerger, Rev. Mod. Phys. **80**, 885 (2008).
[2] O. Guhne and G. Toth, Phys. Rep. **474**, 1 (2009).
[3] V. Giovannetti, S. Lloyd, and L. Maccone, Science **306**, 1330 (2004).
[4] M. Fleischhauer, A. Imamoglu, and J. P. Marangos, Rev. Mod. Phys. **77**, 633 (2005).
[5] L.-M. Duan, M. D. Lukin, J. I. Cirac, and P. Zoller, Nature (London) **414**, 413 (2001).
[6] C. H. van der Wal *et al.*, Science **301**, 196 (2003).
[7] B. Julsgaard, J. Sherson, J. I. Cirac, J. Fiurasek, and E. S. Polzik, Nature (London) **432**, 482 (2004).
[8] D. N. Matsukevich, T. Chanelière, S. D. Jenkins, S.-Y. Lan, T. A. B. Kennedy, and A. Kuzmich, Phys. Rev. Lett. **97**, 013601 (2006).
[9] J. Simon, H. Tanji, J. K. Thompson, and V. Vuletic, Phys. Rev. Lett. **98**, 183601 (2007).
[10] C.-W. Chou *et al.*, Science **316**, 1316 (2007).
[11] B. Zhao *et al.*, Nat. Phys. **5**, 95 (2009).
[12] U. Schnorrberger, J. D. Thompson, S. Trotzky, R. Pugatch, N. Davidson, S. Kuhr, and I. Bloch, Phys. Rev. Lett. **103**, 033003 (2009).
[13] R. Zhao *et al.*, Nat. Phys. **5**, 100 (2009).
[14] N. E. Rehler and J. H. Eberly, Phys. Rev. A **3**, 1735 (1971).
[15] M. Gross and S. Haroche, Phys. Rep. **93**, 301 (1982).
[16] J. P. Clemens, L. Horvath, B. C. Sanders, and H. J. Carmichael, Phys. Rev. A **68**, 023809 (2003).
[17] M. O. Scully, E. S. Fry, C. H. Raymond Ooi, and K. Wódkiewicz, Phys. Rev. Lett. **96**, 010501 (2006).
[18] M. O. Scully and A. A. Svidzinsky, Science **325**, 1510 (2009).
[19] J. H. Eberly, J. Phys. B **39**, S599 (2006).
[20] D. Porras and J. I. Cirac, Phys. Rev. A **78**, 053816 (2008).
[21] R. Wiegner, J. von Zanthier, and G. S. Agarwal, Phys. Rev. A **84**, 023805 (2011).
[22] A. S. Sorensen and K. Molmer, Phys. Rev. Lett. **86**, 4431 (2001).
[23] J. K. Korbicz, O. Gühne, M. Lewenstein, H. Häffner, C. F. Roos, and R. Blatt, Phys. Rev. A **74**, 052319 (2006).
[24] G. Toth, C. Knapp, O. Guhne, and H. J. Briegel, Phys. Rev. Lett. **99**, 250405 (2007).
[25] L.-M. Duan, Phys. Rev. Lett. **107**, 180502 (2011).
[26] M. J. Holland and K. Burnett, Phys. Rev. Lett. **71**, 1355 (1993).
[27] J. Jacobson, G. Bjork, I. Chuang, and Y. Yamamoto, Phys. Rev. Lett. **74**, 4835 (1995).
[28] B. L. Higgins, D. W. Berry, S. D. Bartlett, H. M. Wiseman, and G. J. Pryde, Nature (London) **450**, 393 (2007).
[29] D. Braun and J. Martin, Nat. Commun. **2**, 223 (2011).
[30] E. Altman, E. Demler, and M. D. Lukin, Phys. Rev. A **70**, 013603 (2004).
[31] K. Eckert *et al.*, Nat. Phys. **4**, 50 (2008).
[32] G. M. Bruun, B. M. Andersen, E. Demler, and A. S. Sorensen, Phys. Rev. Lett. **102**, 030401 (2009).
[33] I. de Vega, J. I. Cirac, and D. Porras, Phys. Rev. A **77**, 051804(R) (2008).
[34] T. A. Corcovilos, S. K. Baur, J. M. Hitchcock, E. J. Mueller, and R. G. Hulet, Phys. Rev. A **81**, 013415 (2010).
[35] H. Miyake, G. A. Siviloglou, G. Puentes, D. E. Pritchard, W. Ketterle, and D. M. Weld, Phys. Rev. Lett. **107**, 175302 (2011).
[36] C. Weitenberg, P. Schauß, T. Fukuhara, M. Cheneau, M. Endres, I. Bloch, and S. Kuhr, Phys. Rev. Lett. **106**, 215301 (2011).
[37] K. G. H. Vollbrecht and J. I. Cirac, Phys. Rev. Lett. **98**, 190502 (2007).
[38] M.-K. Zhou, Z.-K. Hu, X.-C. Duan, B.-L. Sun, J.-B. Zhao, and J. Luo, Phys. Rev. A **82**, 061602(R) (2010).
[39] H. J. Carmichael, *An Open Systems Approach to Quantum Optics*, Lecture Notes in Physics, New Series: Monographs, Vol. m18 (Springer, Berlin, 1993).
[40] J. B. Fixler, G. T. Foster, J. M. McGuirk, and M. A. Kasevich, Science **315**, 74 (2007).